Electronic Supplementary Material (ESI) for Physical Chemistry Chemical Physics.

Why do zeolites induce unprecedented electronic state on exchanged metal ions? – Pivotal roles of *Lewis base–metal ion bifunctionality* caused by Al-atoms arrayed circumferentially in the MFI-zeolite pores –

Akira Oda,*[,1,2] Takahiro Ohkubo,[2] Takashi Yumura,[3] Hisayoshi Kobayashi,[3] and Yasushige Kuroda*[,2]

[1]Precursory Research for Embryonic Science and Technology, Japan Science and Technology Agency, 4-1-8 Honcho, Kawaguchi, Saitama 332-0012 (Japan),

[2]Department of Chemistry, Graduate School of Natural Science and Technology, Okayama University, 3-1-1 Tsushima, Kita-ku, Okayama 700-8530 (Japan),

[3]Department of Chemistry and Materials Technology, Kyoto Institute of Technology, Matsugasaki, Sakyo-ku, Kyoto 606-8585 (Japan).

Table S1. Comparisons of natural charges of Zn, O_{jL}, or O_L of the M7-S*N* models.

	M7-S1	M7-S2	M7-S3	M7-S4
Zn	+1.69	+1.69	+1.69	+1.71
O_{jL} or O_L[a]	-1.28	-1.28	-1.29	-1.34

[a] Natural charges of oxygen atoms which act as Lewis base in the heterolytic activation of H_2.

Table S2. Selected structural parameters on the stages (a-d) in the theoretically-reproduced heterolytic H_2 splitting on the M7-S2 model which are shown in Figure 4A and Figure S8.

Bond distance / Å	stage a	stage b	stage c	stage d
Zn-1H	1.924	1.896	1.729	1.519
Zn-2H	1.937	1.937	2.212	3.132
O_{jL}-2H	3.566	3.236	1.500	0.972
1H-2H	0.764	0.770	0.906	2.247
Zn-O_{jL}	3.862	3.681	3.481	3.924

Table S3. Selected structural parameters on the respective states during the theoretically-reproduced heterolytic bond dissociation of H_2 on the M7-S1 model.

Bond distance / Å	Molecularly-adsorption	TS	Dissociative adsorption
Zn-1H	2.124	1.780	1.502
Zn-2H	2.095	2.342	5.104
O_{jL}-2H	3.705	1.405	0.968
1H-2H	0.754	0.926	5.280
Zn-O_{jL}	3.842	3.336	5.096

Table S4. Selected structural parameters on the respective states during the theoretically-reproduced heterolytic bond dissociation of H_2 on the M7-S3 model.

Bond distance / Å	Molecularly-adsorption	TS	Dissociative adsorption
Zn-1H	2.078	1.750	1.502
Zn-2H	2.075	2.407	6.954
O_{jL}-2H	3.088	1.384	0.966
1H-2H	0.757	0.938	7.322
Zn-O_{jL}	3.667	3.449	6.670

Table S5. Selected structural parameters on the respective states during the theoretically-reproduced heterolytic bond dissociation of H_2 on the M7-S4 model.

Bond distance / Å	Molecularly-adsorption	TS	Dissociative adsorption
Zn-1H	2.247	1.687	1.501
Zn-2H	2.218	1.892	4.221
O_{jL}-2H	2.915	1.371	0.966
1H-2H	0.751	0.929	4.174
Zn-O_{jL}	2.074	2.560	3.968

Table S6. ZPE corrected relative energy of the M7-S*N* models.

	M7-S1	M7-S2	M7-S3	M7-S4
ZPE corrected relative energy / kJ mol^{-1}	0	+121	+70	-39

Table S7. ZPE corrected relative energy of the $[M7\text{-}SN]^{2-}$ models which were obtained by removing a Zn^{2+} ion from the respective M7-S*N* models. In the calculation, charges of respective models were set as −2. Similar energy-values were obtained, respectively. This fact indicates the almost energetically-equivalent for all Al arrays. Therefore, significant differences in the relative energy found in respective M7-S*N* models shown in Table S5 are not derived from the difference in the stability of the Al arrays in M7 site, but the stability caused by the Zn-O_L interactions, as discussed in the text.

	$[M7\text{-}S1]^{2-}$	$[M7\text{-}S2]^{2-}$	$[M7\text{-}S3]^{2-}$	$[M7\text{-}S4]^{2-}$
ZPE corrected relative energy / kJ mol^{-1}	0	+18	-11	+17

Table S8. Selected structural parameters on the intermediate geometries in the theoretically-reproduced heterolytic cleavage of H_2 on the M7M5-S1, M7M5-S2, and M7M6-S1 models.

Bond distance / Å	M7M5-S1 Not TS	M7M5-S2 Not TS	M7M6-S1 TS
Zn-1H	1.583	1.648	3.874
Zn-2H	2.124	2.481	5.381
O_L-2H	1.172	1.163	0.998
1H-2H	0.920	0.920	1.900
Zn-O_L	3.047	3.562	6.039

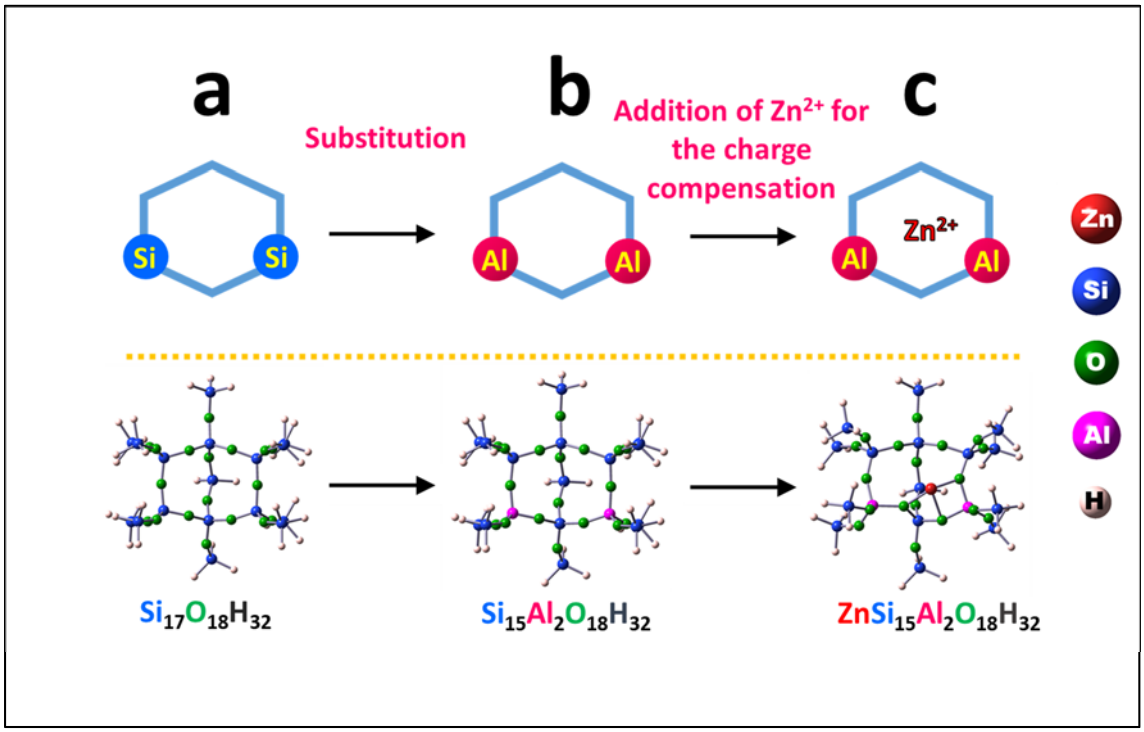

Figure S1. Procedure for constructing the Zn^{2+}-MFI model as a typical example. First, the M7 site was truncated from the MFI structure, followed by the peripheral parts of the truncated model were terminated by H atoms, and only H atoms were optimized (**a**: $Si_{17}O_{18}H_{32}$ cluster). After optimization, two selected Si atoms were substituted for two Al atoms to introduce two negative charges into the zeolite framework (**b**: $Si_{15}Al_2O_{18}H_{32}$ cluster). Subsequently, a Zn^{2+} ion was positioned around two Al atoms. Finally, optimization was carried out on the coordinates of a Zn atom and lattice O atoms (O_L) connected to the respective Al atoms, and the Zn^{2+}-MFI models (**c**: $ZnSi_{15}Al_2O_{18}H_{32}$ cluster) were obtained.

Our calculation methods so far adopted by our group reproduced well the experimental facts as reported in the previous works. Short descriptions on the justification of our system are as follows.

On the use of the H-capped models: In previous works, we have succeeded in creating the unusual states of zinc ions utilizing the reaction field within the sub-nm sized pore of MFI-type zeolite, and characterized these states by various spectroscopic studies coupled with quantum chemical calculation.[1-6] In these processes, in order to verify our claims (the formation of the novel states of zinc ions), we have applied the DFT calculations adopting the truncated MFI models which were constructed by using "*hydrogen-type saturators to satisfy the broken covalent bonds in the peripheral part of the model (between the boundary atoms and the rest of zeolite)*". The H-capped models thus fabricated well explained the experimental facts obtained by our works. Therefore, we can fairly certain that theoretical methods utilizing the H-capped models are adequately useful for the analysis on the phenomena observed in the zinc-ion-exchanged MFI systems.

On the partial optimization methods: In previous works, we have tried to carry out the optimization of all atoms except terminated H atoms, but this procedure leads to significant deformation of the zeolite structure; the final structure took the deformed structure and was far from the valid model. Therefore, we concluded that optimization of all atoms except terminated H atoms is not suitable procedure for analysis on the Zn^{2+} ion-exchanged in MFI, and consequently applied the partial optimization method to avoid the extreme deformation of the zeolite structure. We confirmed that this calculation method explains well the experimental fact regarding to the activation of H_2, CH_4, and CO on a monomeric Zn^{II} ion-exchanged in MFI;[1,3-5] our calculation results are reliable at explaining reasonably the experimental facts. Therefore, we applied our calculation methods and discussed about the experimental facts on the basis of the obtained calculation data.

It is noteworthy that other groups also employed similar methods to reproduce the experimental data regarding to the *local geometry*, *electronic structure*, and *chemical property* of the novel state of the metal ion (active centers) in zeolite[7-10]——these methods had been valid also by other groups.

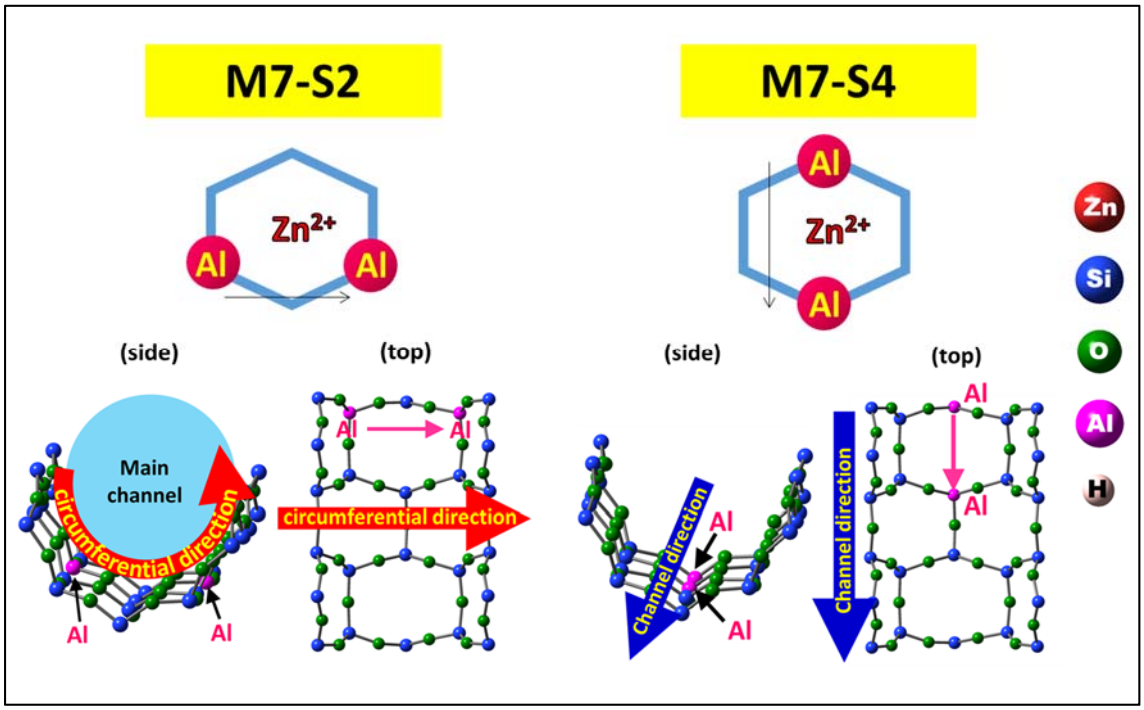

Figure S2. Explanation on the Al-array-direction of the M7-S2 and M7-S4 models: circumferential direction and straight channel direction.

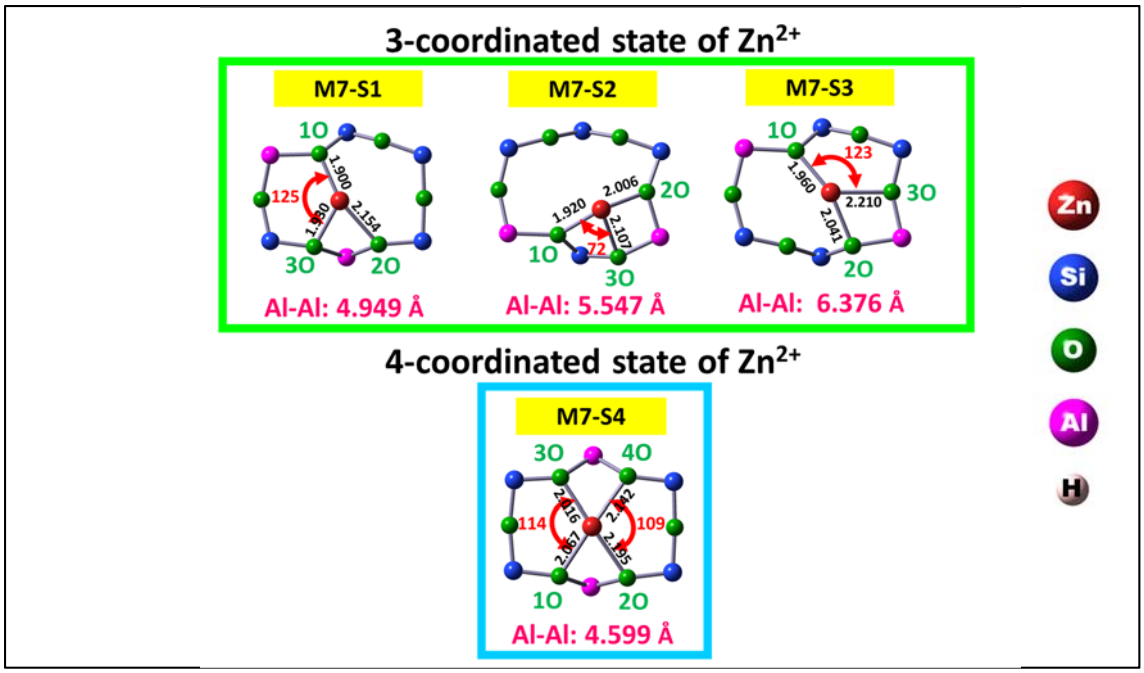

Figure S3. Detailed structural information on the optimized M7-S*N* models (*N*= 1 to 4).

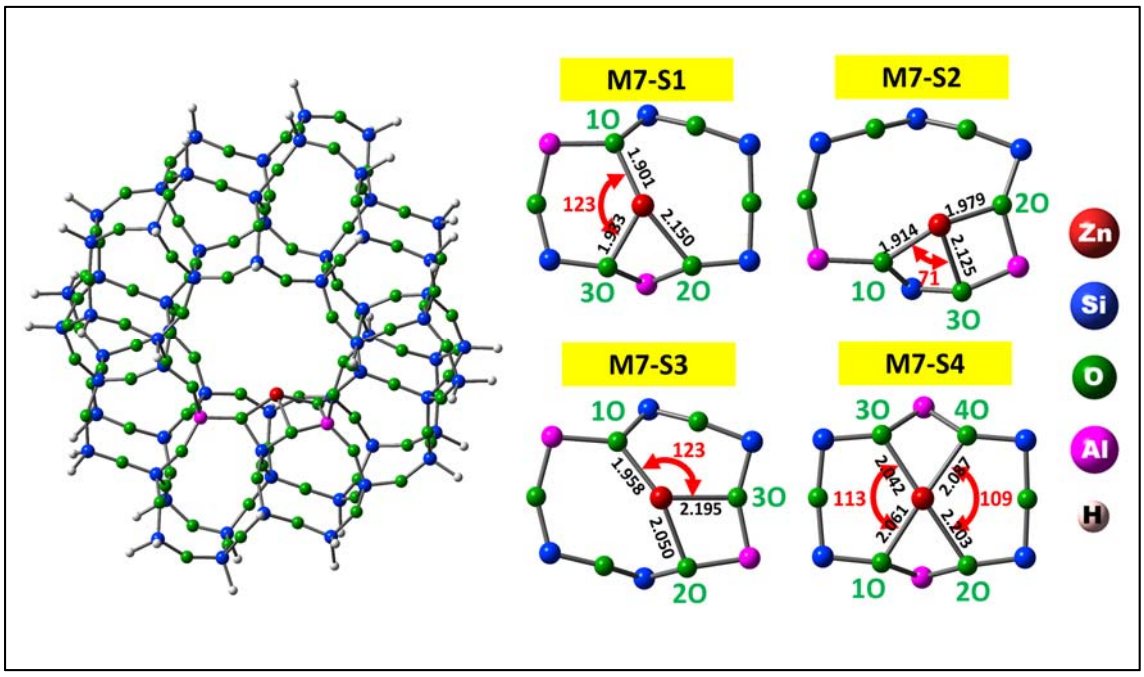

Figure S4. Included in this figure for comparison are the cluster-size dependence of the structures in the M7-S*N* models. The larger cluster model, $ZnSi_{62}Al_2O_{104}H_{48}$, as the MFI-type zeolite was used in this calculation; (left) Optimized M7-S2 model, $ZnSi_{62}Al_2O_{104}H_{48}$ cluster and (right) comparisons of the local geometries of the optimized $ZnSi_{62}Al_2O_{104}H_{48}$ clusters with different Al arrays.

The optimizations were performed by B3LYP/6-311G(d), 6-31G(d) level. In calculation, 6-311G(d) was used for a Zn atom, and 6-31G(d) was used for other atoms. The selected structural parameters, bond distances and a bond angle, were also shown as black and red numbers, respectively.

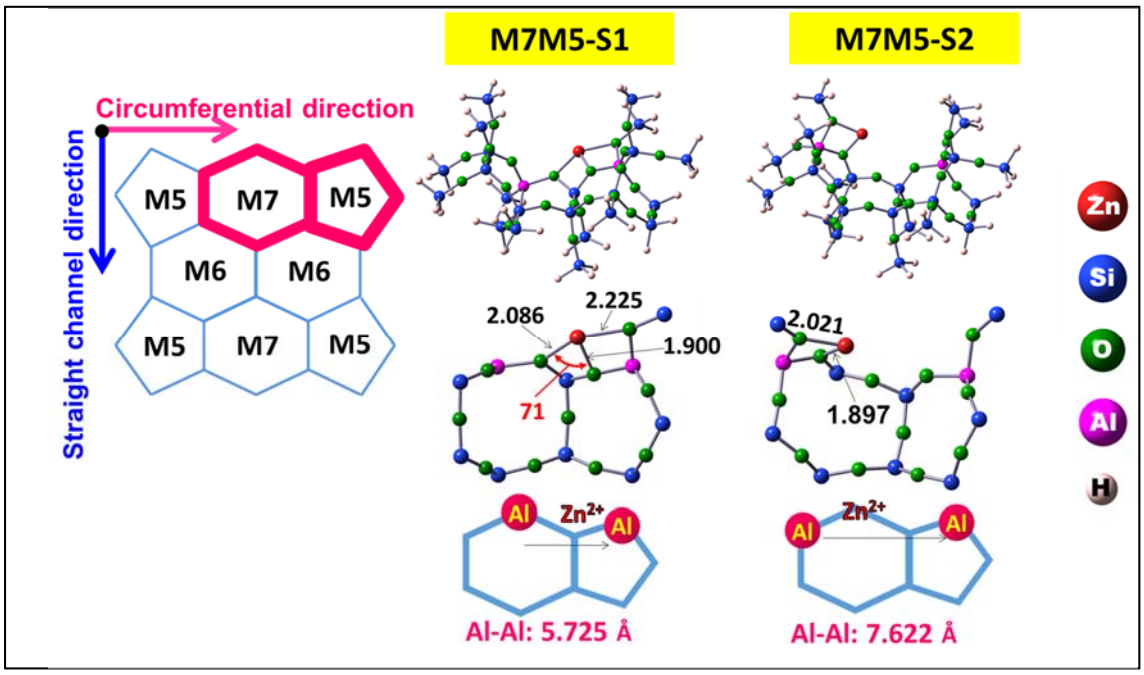

Figure S5. Position of the adjacent M7-M5 site, and the optimized models representing the state of Zn^{2+} ion-exchanged in the adjacent M7-M5 site containing two Al atoms arranged in the circumferential direction with Al-Al distance of 5.725 (M7M5-S1 model) and 7.622 Å (M7M5-S2 models).

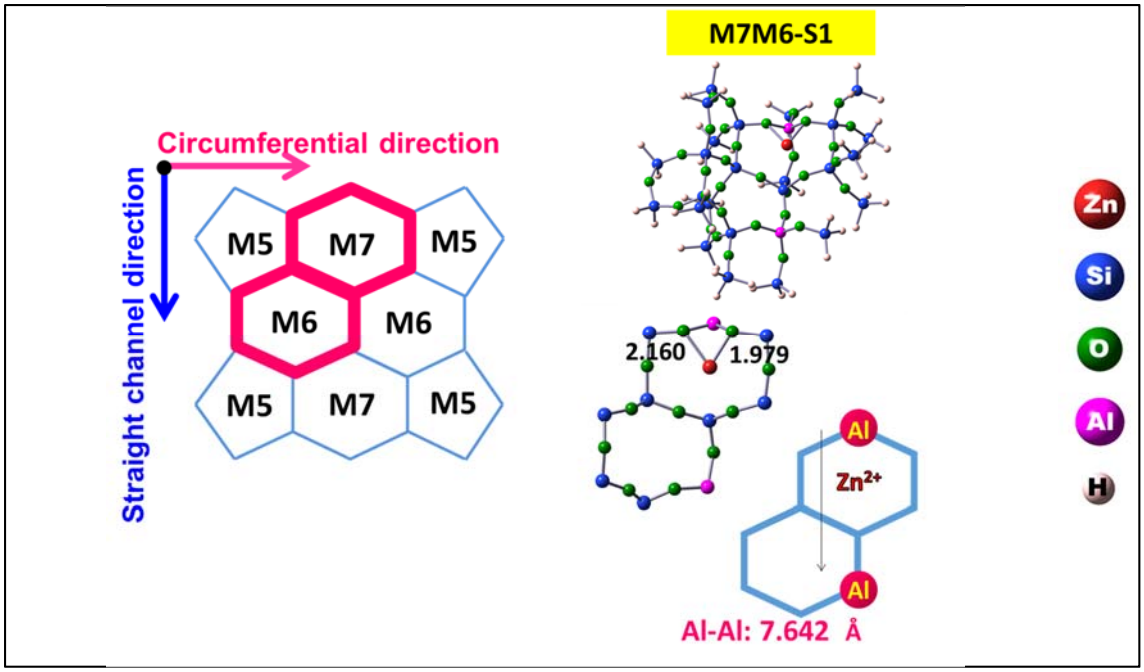

Figure S6. Position of the adjacent M7-M6 site, and the optimized models representing the state of Zn^{2+} ion-exchanged in the adjacent M7-M6 sites containing two Al atoms arranged in the straight channel direction with the Al-Al distance of 7.642 Å.

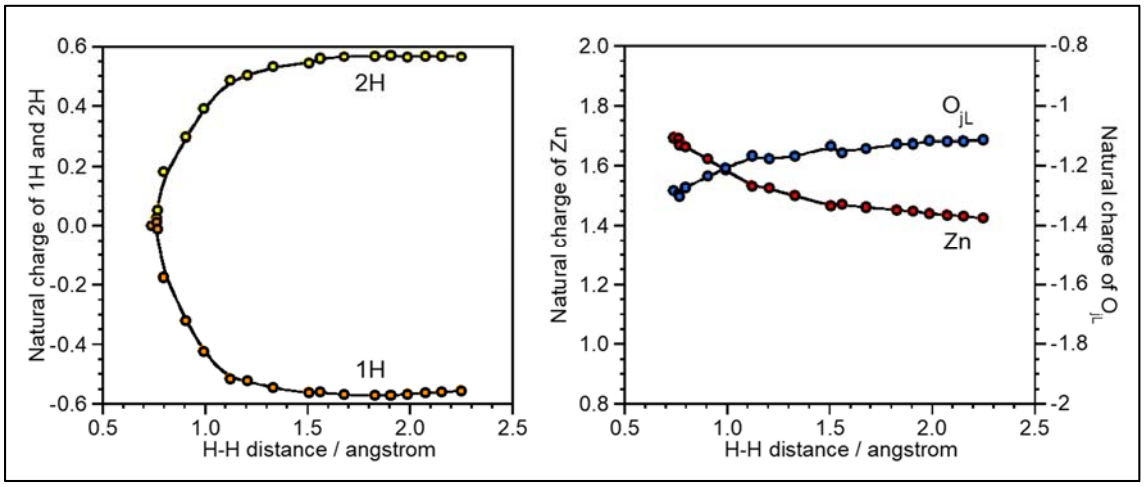

Figure S7. Plots of natural charges of Zn, O_{jL}, 1H, and 2H along the H-H distance during the heterolytic activation of H_2 on the M7-S2 site (see in the text: Figure 4A).

As an H-H bond distance of H_2 molecule gets longer, the natural charge of 2H increases (0.00→+0.57), whereas that of 1H decreases (0.00→-0.56); cationic and anionic hydrogen atoms are formed through the activation process: O_{jL}-$\mathbf{H}^+$ and Zn^{2+}-$\mathbf{H}^-$. On the other hand, the change in the natural charges of Zn and O_{jL} are relatively small, because the process involves neither oxidation nor reduction. These results are well supporting the heterolytic dissociation mechanism.

To gain insights into the site dependency of natural charges of Zn and O_{jL} (or O_L), those of the M7-S*N* models were calculated and compared (**Table S1**). As a result, it was found that strengths of the polarizations induced by Zn^{2+}-O_L Lewis acid pair scarcely depend on the Al array. This indicates that we are unable to explain the site dependency of H_2 activation property of Zn^{2+}-MFI on the basis of the polarization strengths of the active centers; the RT heterolytic activation on Zn^{2+}-MFI originates from other factors such as acid base strengths, and orientation of the intermediate state, as discussed in the text.

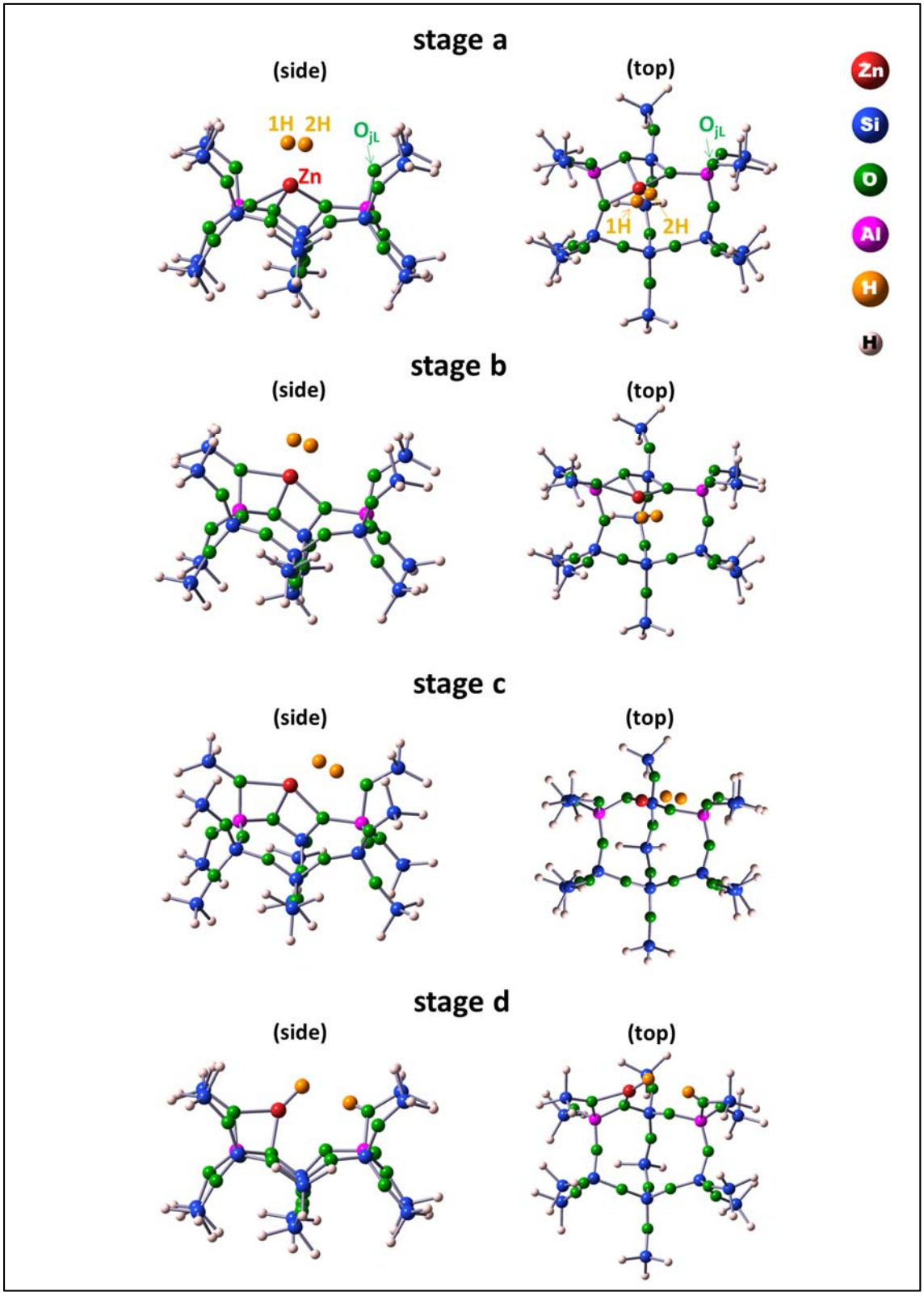

Figure S8. Geometries of the stages a-d on the M7-S2 model shown in Figure 4A.

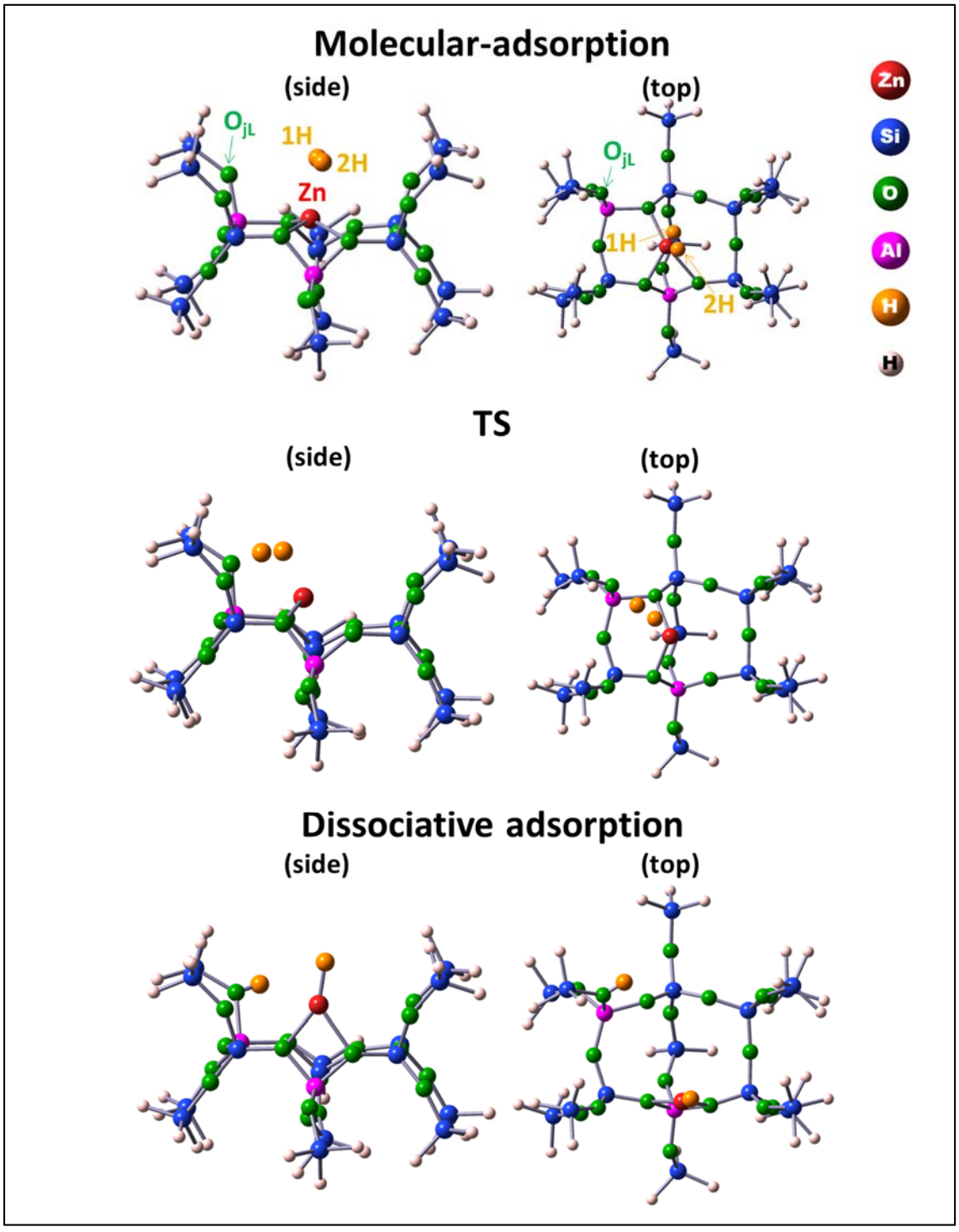

Figure S9. A geometrical change in the heterolytic cleavage of H_2 on the M7-S1 model.

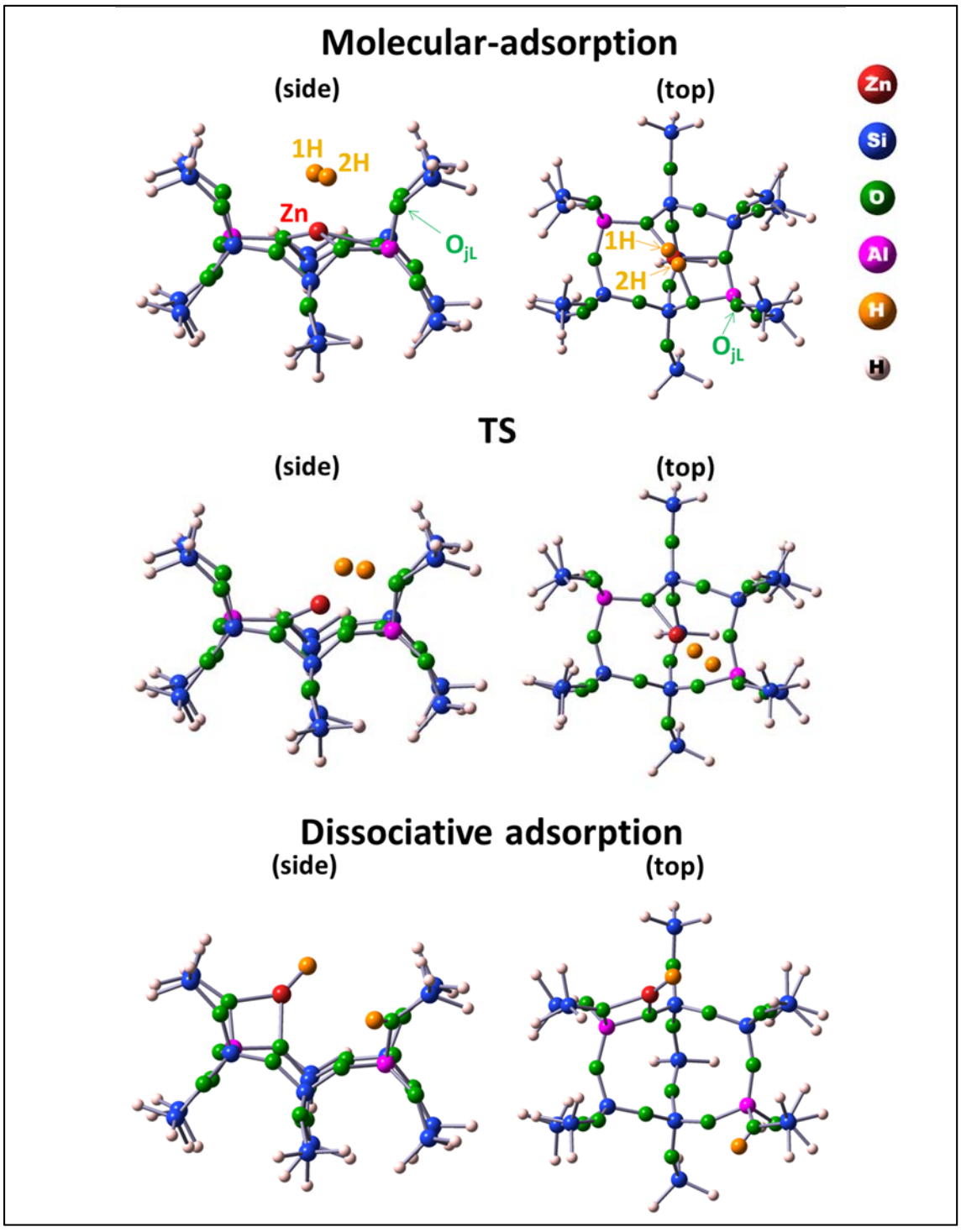

Figure S10. A geometrical change in the heterolytic cleavage of H_2 on the M7-S3 model.

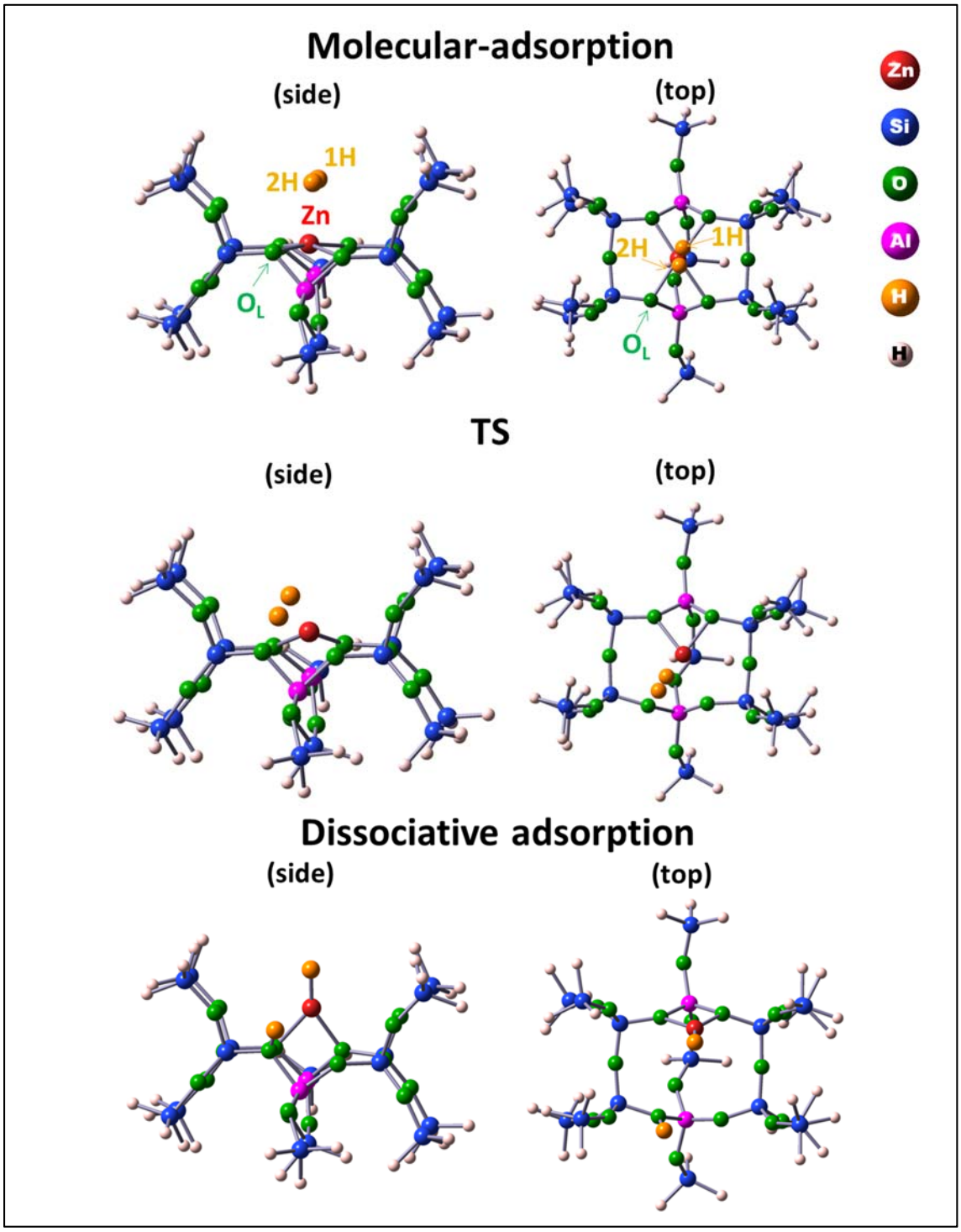

Figure S11. A geometrical change in the heterolytic cleavage of H_2 on the M7-S4 model.

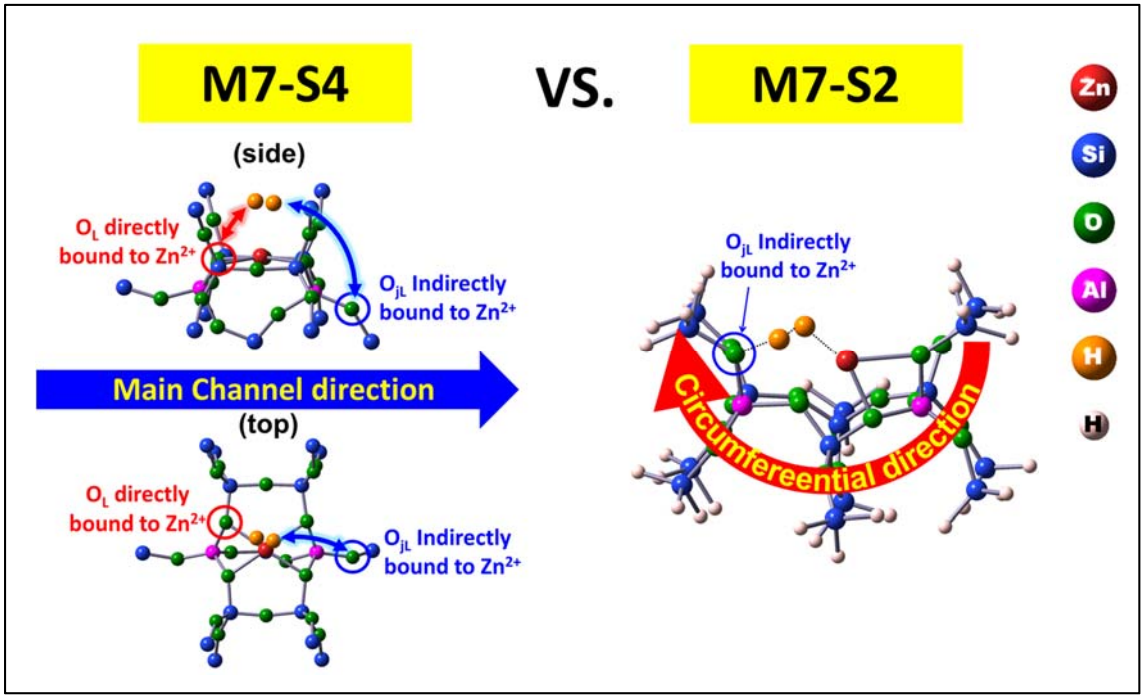

Figure S12. A comparison of the positions of the O_L directly and indirectly bound to Zn^{2+} in the M7-S4 and M7-S2 models. In the M7-S4 model, O_L indirectly bound to Zn^{2+} is positioned not to involve in the H_2 activation due to the lack of the curved feature. On the other hand, in the M7-S2 model (circumferentially-arrayed Al-Al site), O_L indirectly bound to Zn^{2+} (O_{jL}) is positioned to involve in the H_2 activation on the strong acid point (coordinatively-unsaturated and distorted Zn^{2+}) due to the benefit of the curved feature.

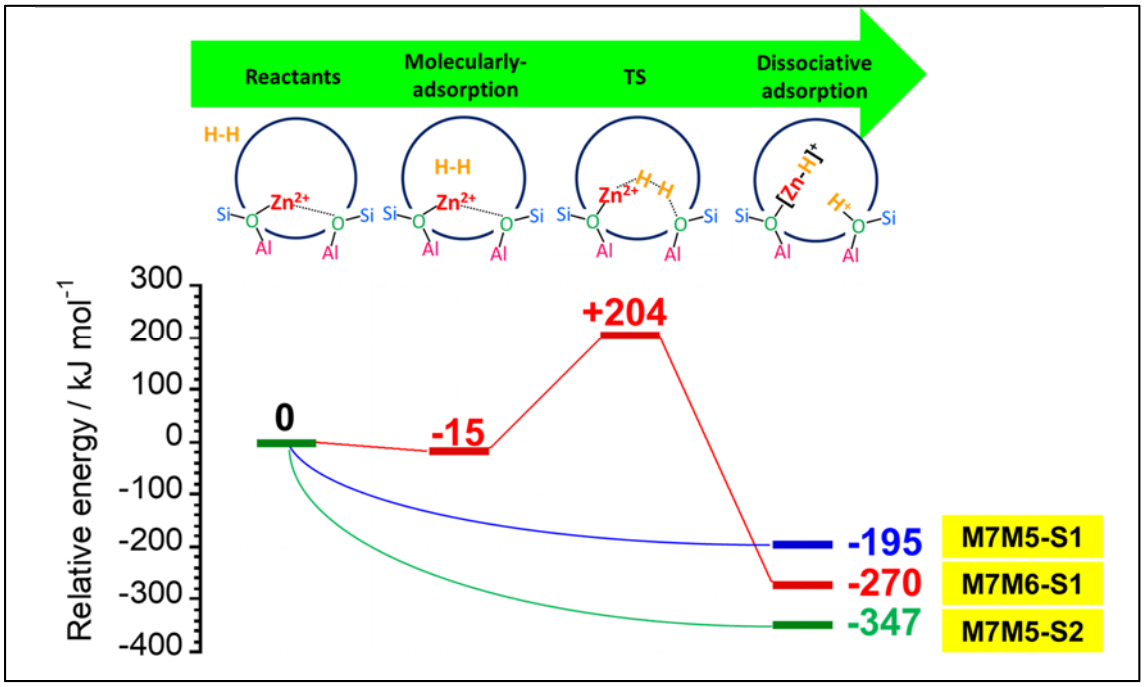

Figure S13. A comparison of the DFT-calculated energy profiles for the heterolytic cleavage of H_2 on the M7M5-S1, M7M5-S2, and M7M6-S1 models. Inserted values mean the relative energy based on the energy of the reactants.

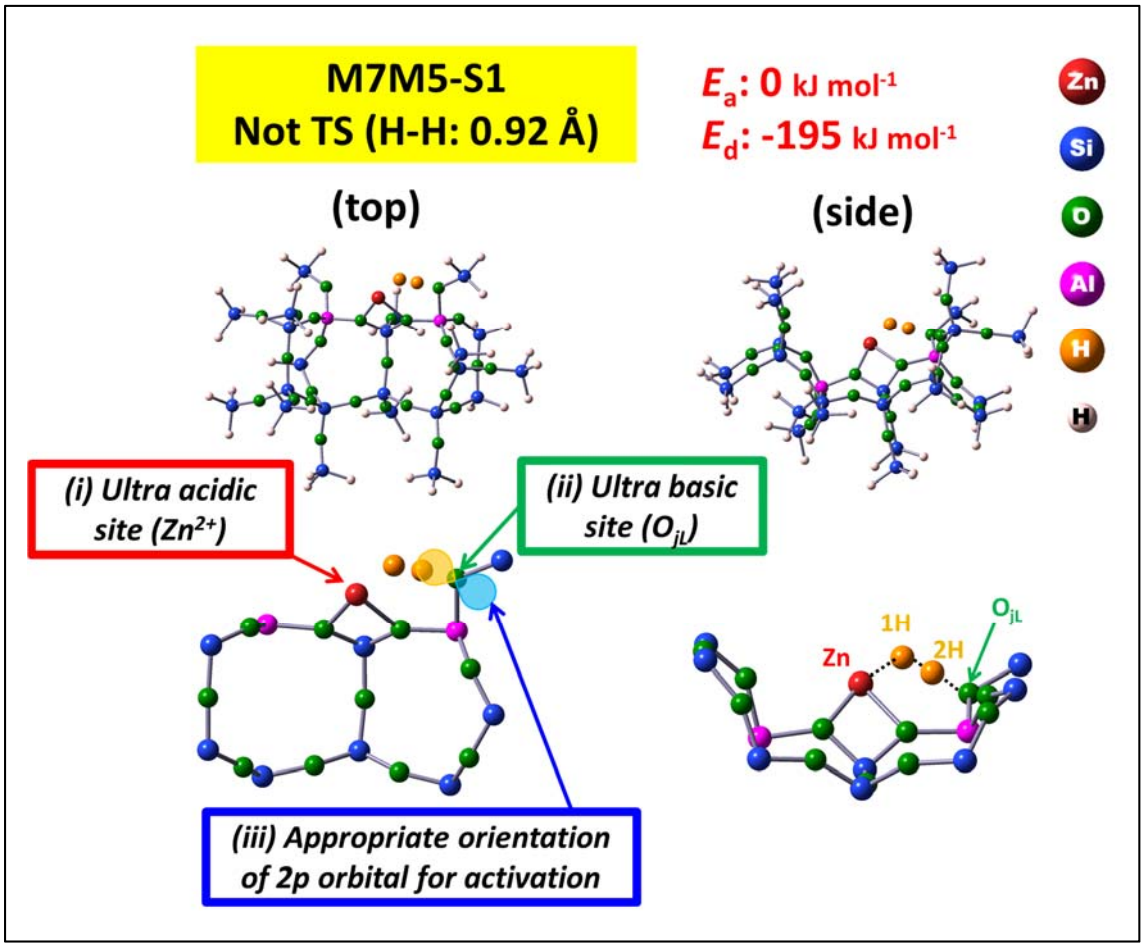

Figure S14. Intermediate geometry with the H-H bond length of 0.92 Å in the theoretically-reproduced heterolytic cleavage of H_2 on the M7M5-S1 model.

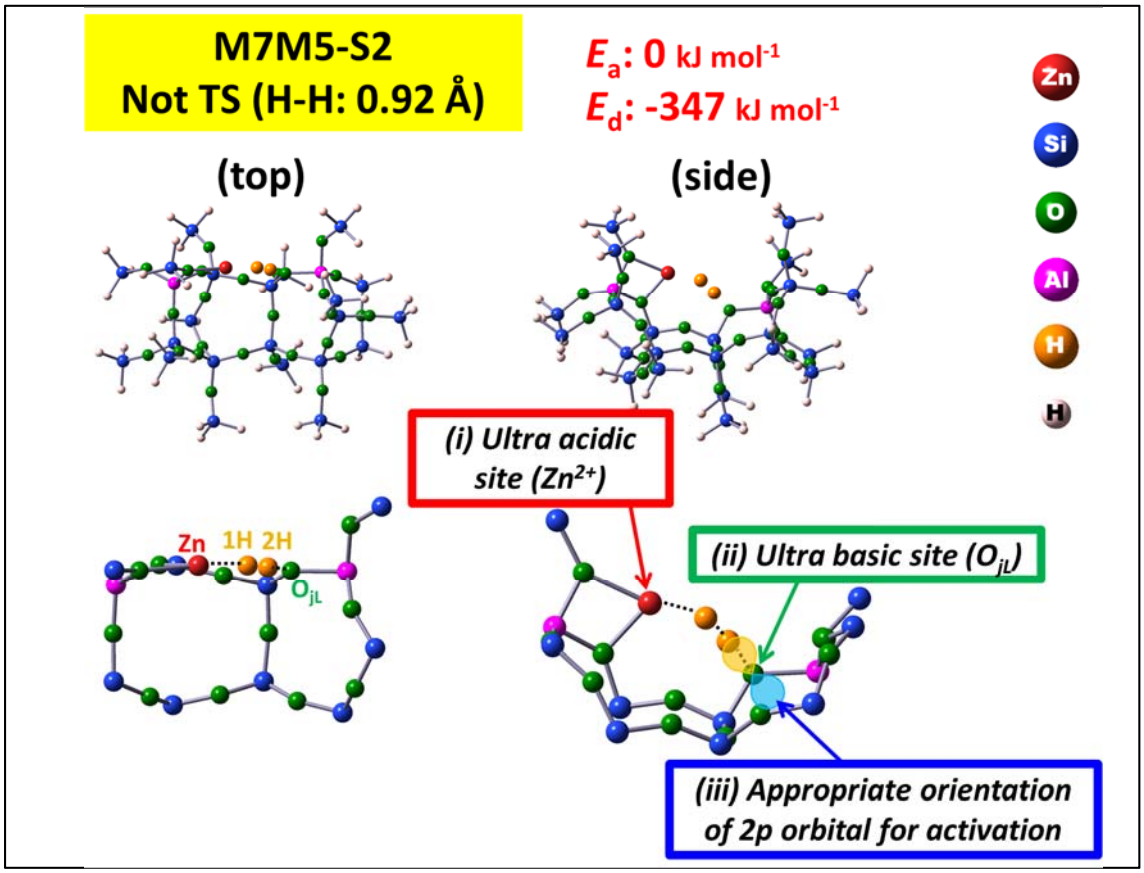

Figure S15. Intermediate geometry with the H-H bond length of 0.92 Å in the theoretically-reproduced heterolytic cleavage of H_2 on the M7M5-S2 model.

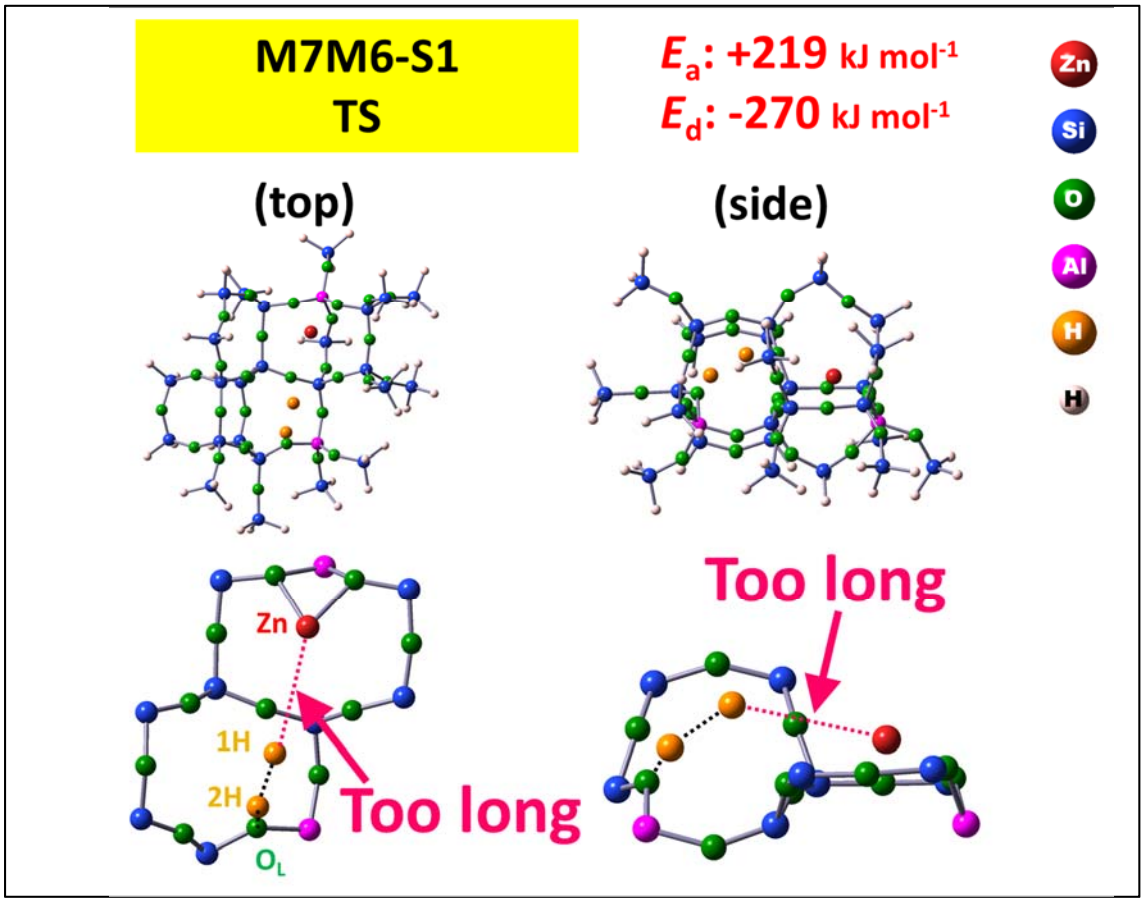

Figure S16. TS geometry for the theoretically-reproduced heterolytic cleavage of H_2 on the M7M6-S1 model.

References

[1] A. Oda, H. Torigoe, A. Itadani, T. Ohkubo, T. Yumura, H. Kobayashi, Y. Kuroda, *Angew. Chem. Int. Ed.*, 2012, **51**, 7719.

[2] A. Oda, H. Torigoe, A. Itadani, T. Ohkubo, T. Yumura, H. Kobayashi, Y. Kuroda, *J. Am. Chem. Soc.*, 2013, **135**, 18481.

[3] A. Oda, H. Torigoe, A. Itadani, T. Ohkubo, T. Yumura, H. Kobayashi, Y. Kuroda, *J. Phys. Chem. C*, 2013, **117**, 19525.

[4] A. Oda, H. Torigoe, A. Itadani, T. Ohkubo, T. Yumura, H. Kobayashi, Y. Kuroda, *J. Phys. Chem. C*, 2014, **118**, 15234.

[5] A. Oda, T. Ohkubo, T. Yumura, H. Kobayashi, Y. Kuroda, *Dalton Trans.*, 2015, **44**, 10038.

[6] A. Oda, T. Ohkubo, T. Yumura, H. Kobayashi, Y. Kuroda, *Angew. Chem. Int. Ed.*, 2017, **56**, 9715.

[7] P. Pietrzyk, K. Podolska, T. Mazur, Z. Sojka, *J. Am. Chem. Soc.*, 2011, **133**, 19931.

[8] P. Pietrzyk, T. Mazur, K. Podolska-Serafin, M. Chiesa, Z. Sojka, *J. Am. Chem. Soc.*, 2013, **135**, 15467.

[9] M.-L. Tsai, R. G. Hadt, P. Vanelderen, B. F. Sels, R. A. Schoonheydt, E. I. Solomon, *J. Am. Chem. Soc.*, 2014, **136**, 3522.

[10] B. E. R. Snyder, P. Vanelderen, M. L. Bols, S. D. Hallaert, L. H. Böttger, L. Ungur, K. Pierloot, R. A. Schoonheydt, B. F. Sels, E. I. Solomon, *Nature*, 2016, **536**, 317.